

# A BOUNDARY-TYPE MESHLESS METHOD FOR ANALYSIS OF THIN STRUCTURES

Zhang Jianming<sup>1)</sup>, Yao Zhenhan<sup>2)</sup>, Masataka Tanaka<sup>3)</sup>

1) Faculty of Engineering, Shinshu University, Nagano 380-8553, Email: [zhangjim@homer.shinshu-u.ac.jp](mailto:zhangjim@homer.shinshu-u.ac.jp)

2) Department of Engineering Mechanics, Tsinghua University, Beijing 100084, Email: [demyzh@tsinghua.edu.cn](mailto:demyzh@tsinghua.edu.cn)

3) Faculty of Engineering, Shinshu University, Nagano 380-8553, Email: [dtanaka@gipwc.shinshu-u.ac.jp](mailto:dtanaka@gipwc.shinshu-u.ac.jp)

Thin structures are generally solved by the Finite Element Method (FEM), using plate or shell finite elements which have many limitations in applications, such as numerical locking, length scaling and the convergence problem. Recently, by proposing a new approach of treating the nearly-singular integrals, Liu et al. developed a BEM to successfully solve thin structures with the thickness-to-length ratios in the nano-scale. On the other hand, the meshless Regular Hybrid Boundary Node Method (RHBNM), which is proposed by the current authors and based on a modified functional and the Moving Least-Square (MLS) approximation, has very promising applications for engineering problems due to its meshless nature and dimension-reduction advantage. Test examples, presented in this paper, show that the RHBNM can also be applied readily to thin structures with high accuracy.

**Keywords:** meshless, moving least squares approximation, hybrid boundary node method.

## 1. Introduction

The finite element method (FEM) has been a successful tool for the analysis of shell structures in engineering using shell elements. The shell elements are based on shell theory in which many assumptions about the geometry, loading and deformation of the structure are introduced when a 3-D body is abstracted into a 2-D model. Therefore, various pitfalls are also introduced, such as numerical locking, length scaling and especially the convergence problem, and these limit the FEM in applications in many ways. It is advantageous and desirable to turn to 3-D elasticity theory in building numerical models for shell-like structures, which have non-uniform thicknesses or are linked to bulky solids, in a unified formulation. Unfortunately, this has not been achieved in the FEM using shell theory, though a great deal of research effort has been made in the last three decades. Recently, by proposing a new approach of treating nearly-singular integrals, Liu et al. [1,2] successfully developed the BEM to solve thin structures with the thickness-to-length ratios in the nano-scale.

Meshless methods are gaining popularity ever since the publication of the element free Galerkin (EFG) method by Belytschko et al. [3], in which though no mesh is required for the interpolation of the solution variables, background cells are inevitable for the integration of 'energy'. In 1998, two meshless methods, the Meshless Local Boundary Integral Equation (MLBIE) method by Zhu et al. [4] and the Meshless Local Petrov-Galerkin (MLPG) approach by Atluri et al. [5] have been developed. Both methods use local weak forms over a local sub-domain and shape functions from the MLS approximation, and lead to truly

meshless ones. In 1997, Mukherjee et al. [6] combined the MLS with Boundary Integral Equations (BIE) to achieve a boundary-type meshless method which they called Boundary Node Method (BNM). This method is not a truly meshless one yet, as an underlying cell structure is inevitable for numerical integration.

To achieve a truly boundary-type meshless method, a Hybrid Boundary Node Method (Hybrid BNM) was introduced by Zhang et al. [7], based on the MLS interpolation scheme and the hybrid displacement variational formulation. In this method, only scattered nodes are needed to be constructed on boundary of the domain. However, the HBNM has a drawback of "boundary layer effect", i.e. the accuracy of results in the vicinity of the boundary is very sensitive to the proximity of the interior points to the boundary. To avoid this pitfall, a new meshless Regular Hybrid Boundary Node Method (RHBNM) [8] has been proposed, in which the source points of the fundamental solutions are located outside the domain rather than at the boundary nodes as in the Hybrid BNM or other hybrid boundary element models.

The RHBNM does not involve any singular or nearly-singular integration, so it is possibly viable to thin structures. In this paper, several test examples are presented to demonstrate the effectiveness and high accuracy of the RHBNM in the analyses of the very thin structures, some of which are even in the nano-scales, as in [1,2].

## 2. The MLS approximation scheme for the 2-D RHBNM

This section gives a brief summary of the MLS approximation, of which excellent illustrations can be seen in Reference [3].

In the view of the fact that this MLS interpolation scheme will be coupled later with 2-D hybrid displacement variational formulation which uses three independent variables, i.e. displacement  $u_i$  in the domain, displacement  $\tilde{u}_i$  and traction  $\tilde{t}_i$ ,  $i=1,2$ , on the boundary, of which the  $\tilde{u}_i$  and  $\tilde{t}_i$  will be interpolated by MLS scheme. The discussion below use the variables  $\tilde{u}$  and  $\tilde{t}$  to represent any particular component of the displacement and traction respectively, for the sake of brevity of index notation.

In contrast to the BNM, the MLS interpolation in the present approach is independently performed on piecewise smooth segments  $\Gamma_i$ ,  $i=1,2,\dots,n$  which constitute the boundary naturally other than on the whole boundary  $\Gamma$ . To approximate the functions  $\tilde{u}$  and  $\tilde{t}$  on each  $\Gamma_i$  over which a number of nodes  $\{s_I\}$ ,  $I=1,2,\dots,N$ , are randomly located, the MLS interpolants for  $\tilde{u}$  and  $\tilde{t}$  are defined as

$$\tilde{u}(s) = \sum_{j=1}^m p_j(s) a_j(s) = \mathbf{p}^T(s) \mathbf{a}(s) \quad (1)$$

$$\tilde{t}(s) = \sum_{j=1}^m p_j(s) b_j(s) = \mathbf{p}^T(s) \mathbf{b}(s) \quad (2)$$

where  $s$  is a curvilinear co-ordinate on  $\Gamma_i$ ,  $p_1=1$  and  $p_j(s)$ ,  $j=2,\dots,m$  are monomials in  $s$ . In this paper, a quadratic background basis is used, i.e.

$$\mathbf{p}^T(s) = [1, s, s^2], \quad m = 3 \quad (3)$$

The coefficient vector  $\mathbf{a}(s)$  and  $\mathbf{b}(s)$  is determined by minimizing a weighted discrete  $L_2$  norm, defined as

$$J_1(s) = \sum_{I=1}^N w_I(s) [\mathbf{p}^T(s_I) \mathbf{a}(s) - \hat{u}_I]^2 \quad (4)$$

$$J_2(s) = \sum_{I=1}^N w_I(s) [\mathbf{p}^T(s_I) \mathbf{b}(s) - \hat{t}_I]^2 \quad (5)$$

where points  $s_I$  are boundary nodes on  $\Gamma_i$ ;  $s$  is the co-ordinate of an evaluation point  $E$  on  $\Gamma_i$ ;  $N$  is the number of boundary nodes in the neighborhood of  $E$  for which the weight functions  $w(s-s_I) > 0$ .

Solving for  $\mathbf{a}(s)$  and  $\mathbf{b}(s)$  by minimizing  $J_1$  and  $J_2$  in equation (4) and (5), and substituting them into equation (1) and (2) gives a relation which may be written as the form of an interpolation function similar to that used in the FEM, as

$$\tilde{u}(s) = \sum_{I=1}^N \Phi_I(s) \hat{u}_I \quad (6)$$

$$\tilde{t}(s) = \sum_{I=1}^N \Phi_I(s) \hat{t}_I \quad (7)$$

where

$$\Phi_I(s) = \sum_{j=1}^m p_j(s) [A^{-1}(s) B(s)]_{ji} \quad (8)$$

with the matrices  $A(s)$  and  $B(s)$  being defined by

$$A(s) = \sum_{I=1}^N w_I(s) \mathbf{p}(s_I) \mathbf{p}^T(s_I) \quad (9)$$

$$B(s) = [w_1(s) \mathbf{p}(s_1), w_2(s) \mathbf{p}(s_2), \dots, w_N(s) \mathbf{p}(s_N)] \quad (10)$$

The MLS approximation is well defined only when the matrix  $A$  in equation (9) is non-singular.

Several kinds of weight function can be seen in the literatures. Gaussian weight function corresponding to node  $s_I$  may be written as

$$w_I(s) = \begin{cases} \frac{\exp[-(d_I/c_I)^2] - \exp[-(\hat{d}_I/c_I)^2]}{1 - \exp[-(\hat{d}_I/c_I)^2]}, & 0 \leq d_I \leq \hat{d}_I \\ 0, & d_I \geq \hat{d}_I \end{cases} \quad (11)$$

where  $d_I = |s - s_I|$ , the absolute value of the distance between an evaluation point and a node, measured along  $\Gamma_i$ ,  $c_I$  is a constant controlling the shape of the weight function, and  $\hat{d}_I$  is the size of the support for the weight function  $w_I$  and determines the support of node  $s_I$ . The  $\hat{d}_I$  should be chosen such that  $\hat{d}_I$  should be large enough to have sufficient number of nodes covered in the domain of definition of every sample point ( $N \geq m$ ) to ensure the regularity of  $A$ .

### 3. Development of the Regular Hybrid Boundary Node method

The development of the RHBNM is illustrated by the following 2-D elasticity problem:

$$\begin{aligned} \sigma_{ij,j} + b_j &= 0, & \forall x \in \Omega \\ u_i &= \bar{u}_i, & \forall x \in \Gamma_u \\ t_i &\equiv \sigma_{ij} n_j = \bar{t}_i, & \forall x \in \Gamma_t \end{aligned} \quad (12)$$

where the domain  $\Omega$  is enclosed by  $\Gamma = \Gamma_u + \Gamma_t$ ;  $\bar{u}_i$  and  $\bar{t}_i$  are the prescribed displacements and tractions, respectively,

on the essential boundary  $\Gamma_u$  and on the traction boundary  $\Gamma_t$ ; and  $n$  is the outward normal direction to the boundary  $\Gamma$ , with  $n_i$  components.

The hybrid boundary model proposed here is based on a modified variational principle. The functions to be independent are:

- displacement field in the domain,  $\mathbf{u}$ , with  $u_i$  components;
- boundary displacement field,  $\tilde{\mathbf{u}}$ , with  $\tilde{u}_i$  components;
- boundary tractions,  $\tilde{\mathbf{t}}$ , with  $\tilde{t}_i$  components.

The corresponding variational functional,  $\Pi_{HB}$ , is defined as in the hybrid BEM model by DeFigueredo and Brebbia [9]:

$$\begin{aligned} \Pi_{AB} = & \int_{\Omega} \left( \frac{1}{2} u_{i,j} C_{ijkl} u_{k,l} - b_i u_i \right) d\Omega \\ & - \int_{\Gamma} \tilde{t}_i (u_i - \tilde{u}_i) d\Gamma - \int_{\Gamma} \tilde{t}_i \tilde{u}_i d\Gamma \end{aligned} \quad (13)$$

In the above equation, the boundary displacement  $\tilde{u}_i$  satisfies the essential boundary conditions, i.e.,  $\tilde{u}_i = \bar{u}_i$  on  $\Gamma_u$ . By carrying out the variations it can be shown that:

$$\begin{aligned} \delta \Pi_{AB} = & \int_{\Omega} (-\sigma_{ij,j} - b_i) \delta u_i d\Omega + \int_{\Gamma} (t_i - \tilde{t}_i) \delta u_i d\Gamma - \\ & \int_{\Gamma} (u_i - \tilde{u}_i) \delta \tilde{t}_i d\Gamma - \int_{\Gamma} (\tilde{t}_i - \bar{t}_i) \delta \tilde{u}_i d\Gamma \end{aligned} \quad (14)$$

where  $\sigma_{ij}$  and  $t_i$  are the stress tensor and the traction vector, respectively.

With the vanishing of  $\delta \Pi_{AB}$ , the following equivalent integral equations can be obtained:

$$\int_{\Gamma} (t_i - \tilde{t}_i) \delta u_i d\Gamma - \int_{\Omega} (\sigma_{ij,j} + b_j) \delta u_i d\Omega = 0 \quad (15)$$

$$\int_{\Gamma} (u_i - \tilde{u}_i) \delta \tilde{t}_i d\Gamma = 0 \quad (16)$$

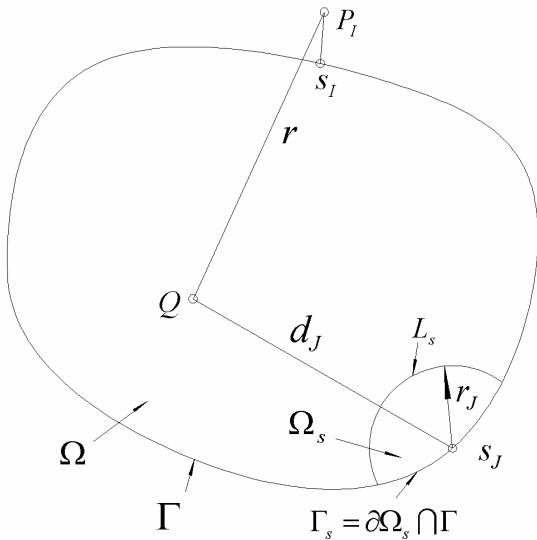


Figure 1: The local domain  $\Omega_s$  and the source point  $P_l$ .

It can be seen that the equation (15) and (16) holds also in the sub-domain  $\Omega_s$  and its boundary  $\Gamma_s$  and  $L_s$  (where  $\Omega_s$  is the intersection of the domain  $\Omega$  and a circle centered at a boundary node  $s_j$ , see Figure 1). Therefore, we can use the following weak forms on the sub-domain  $\Omega_s$ :

$$\int_{\Gamma_s + L_s} (t_i - \tilde{t}_i) v d\Gamma - \int_{\Omega_s} (\sigma_{ij,j} + b_i) v d\Omega = 0 \quad (17)$$

$$\int_{\Gamma_s + L_s} (u_i - \tilde{u}_i) v d\Gamma = 0 \quad (18)$$

In equation (17) and (18),  $\tilde{u}$  and  $\tilde{q}$  on  $\Gamma_s$  are expressed equations (6) and (7). Further, we deliberately select the test function,  $v$ , as the weight function in the MLS approximation with the radius  $\hat{d}_i$  of the support of the weight function being replaced by the radius  $r_j$  of the sub-domain  $\Omega_s$ , i.e.

$$v_j(Q) = \begin{cases} \frac{\exp[-(d_j/c_j)^2] - \exp[-(r_j/c_j)^2]}{1 - \exp[-(r_j/c_j)^2]}, & r_j \geq d_j \geq 0 \\ 0, & d_j \geq r_j \end{cases} \quad (19)$$

where  $d_j$  is the distance between a point  $Q$ , in the domain  $\Omega$ , and the nodal point  $s_j$ . Thus  $v$  equals zero on  $L_s$ , and hence all integrals on  $L_s$  vanish.

The  $\mathbf{u}$  and  $\mathbf{t}$  inside  $\Omega$  are defined as

$$\mathbf{u} = \begin{Bmatrix} u_1 \\ u_2 \end{Bmatrix} = \sum_{I=1}^{NN} \begin{bmatrix} u_{11}^I & u_{12}^I \\ u_{21}^I & u_{22}^I \end{bmatrix} \begin{Bmatrix} x_1^I \\ x_2^I \end{Bmatrix} \quad (20)$$

$$\mathbf{t} = \begin{Bmatrix} t_1 \\ t_2 \end{Bmatrix} = \sum_{I=1}^{NN} \begin{bmatrix} t_{11}^I & t_{12}^I \\ t_{21}^I & t_{22}^I \end{bmatrix} \begin{Bmatrix} x_1^I \\ x_2^I \end{Bmatrix} \quad (21)$$

where  $u_{ij}^I$  and  $t_{ij}^I$  is the fundamental solution with source point at a point  $P_I$ , which locates at the outside of the domain and is corresponding to a node  $s_I$ ;  $x_i^I$  are unknown parameters;  $NN$  is the total number of boundary nodes.

For 2-D elasticity problem, the fundamental solution is

$$\begin{aligned} u_{ij}^I &= \frac{-1}{8\pi(1-\nu)G} \left[ (3-4\nu)\delta_{ij} \ln(r) - r_i r_j \right] \\ t_{ij}^I &= \frac{-1}{4\pi(1-\nu)r} \left\{ [(1-2\nu)\delta_{ij} + 2r_i r_j] \frac{\partial r}{\partial n} + (1-2\nu)(r_i n_j - r_j n_i) \right\} \end{aligned} \quad (22)$$

where  $r(P_I, Q) = \sqrt{(x(Q) - x(P_I))^2 + (y(Q) - y(P_I))^2}$ ;  $Q$  and  $P_I$  are field point and source point respectively. And  $P_I$  is determined by

$$\mathbf{P}_I = \mathbf{s}_I + h \cdot SF \cdot \mathbf{n}(\mathbf{s}_I) \quad (23)$$

where  $h$  is the mesh size;  $\mathbf{n}(\mathbf{s}_j)$  is the outward normal direction to the boundary at node  $\mathbf{s}_j$ ; and  $SF$  is a scale factor.

As  $\mathbf{u}$  is expressed by equation (11), the term  $\sigma_{ij,j}$  in the left hand in equation (6) vanishes. By substituting equation (6), (7), (19), (20) and (21) into equation (17) and (18), and omitting the vanished terms and the body force, we have:

$$\begin{aligned} & \sum_{I=1}^{NN} \int_{\Gamma_s} \begin{bmatrix} u_{11}^I & u_{12}^I \\ u_{21}^I & u_{22}^I \end{bmatrix} \begin{Bmatrix} x_1^I \\ x_2^I \end{Bmatrix} v_J(Q) d\Gamma \\ &= \sum_{I=1}^{NN} \int_{\Gamma_s} \begin{bmatrix} \Phi_I(s) & 0 \\ 0 & \Phi_I(s) \end{bmatrix} \begin{Bmatrix} \hat{u}_1^I \\ \hat{u}_2^I \end{Bmatrix} v_J(Q) d\Gamma \\ & \sum_{I=1}^{NN} \int_{\Gamma_s} \begin{bmatrix} t_{11}^I & t_{12}^I \\ t_{21}^I & t_{22}^I \end{bmatrix} \begin{Bmatrix} x_1^I \\ x_2^I \end{Bmatrix} v_J(Q) d\Gamma \\ &= \sum_{I=1}^{NN} \int_{\Gamma_s} \begin{bmatrix} \Phi_I(s) & 0 \\ 0 & \Phi_I(s) \end{bmatrix} \begin{Bmatrix} \hat{t}_1^I \\ \hat{t}_2^I \end{Bmatrix} v_J(Q) d\Gamma \end{aligned} \quad (24)$$

Using the above equations for all nodes, we can get the final system of equations:

$$\mathbf{U}\mathbf{x} = \mathbf{H}\hat{\mathbf{u}} \quad (25)$$

$$\mathbf{T}\mathbf{x} = \mathbf{H}\hat{\mathbf{t}} \quad (26)$$

where

$$U_{IJ} = \int_{\Gamma_s^J} \begin{bmatrix} u_{11}^I & u_{12}^I \\ u_{21}^I & u_{22}^I \end{bmatrix} v_J(Q) d\Gamma$$

$$T_{IJ} = \int_{\Gamma_s^J} \begin{bmatrix} t_{11}^I & t_{12}^I \\ t_{21}^I & t_{22}^I \end{bmatrix} v_J(Q) d\Gamma$$

$$H_{IJ} = \int_{\Gamma_s^J} \begin{bmatrix} \Phi_I(s) & 0 \\ 0 & \Phi_I(s) \end{bmatrix} v_J(Q) d\Gamma$$

$$\mathbf{x}^T = [x_1^1, x_2^1, \dots, x_1^N, x_2^N]$$

$$\hat{\mathbf{t}}^T = [\hat{t}_1^1, \hat{t}_2^1, \dots, \hat{t}_1^N, \hat{t}_2^N]$$

$$\hat{\mathbf{u}}^T = [\hat{u}_1^1, \hat{u}_2^1, \dots, \hat{u}_1^N, \hat{u}_2^N]$$

For a well-posed problem, values of either  $u_i$  or  $t_i$  are known at each node on the boundary, Therefore, by rearranging the governing equations (25) and (26), we obtain the final system in term of  $\mathbf{x}$  only, and the unknown vector  $\mathbf{x}$  is obtained by solving the final equations system. Displacements  $u_i$  and tractions  $t_i$  at any point inside domain  $\Omega$  or on boundary  $\Gamma$  are evaluated by equation (20) and (21) without further integrations.

From the above development, one can see that the present method is not merely a truly meshless one, but also a regular one, as no singular integrals or nearly-singular integrals are

involved. So it may be used to solve thin shell-like structure problems.

#### 4. Numerical verifications

To verify the RHBNM for thin structure problems, three test examples are studied in this section, together with comparisons with exact solutions (if it is available). In all examples, the size of the local domain (radius  $r_j$ ) for each node is chosen as  $1.0h$  in all computations and the parameter  $c_j$  in equation (10) is taken to be such that  $r_j/c_j$  is constant and equal to 4.0. The scale factor ( $SF$ ) in equations (14) for the first example is taken to be 7.0 and for the next two examples to be 3.0. Also, in all integrations, 5 Gauss points are used on each of the two half-parts of  $\Gamma_s$ .

##### 4.1 Test problem 1: Displacement field problem on an ellipse

The geometry of this problem is shown in Figure 2. The half-length of the major axis  $a$  is kept constant in this study, while the half-length of the minor axis  $b$  changes from  $1.0a$  to  $1.0 \times 10^{-6}a$ . This setup, therefore, provides a model of the ellipse which can be categorized as a thin shell, a thick shell and even a bulky solid, according to the values of the ratio  $b/a$ .

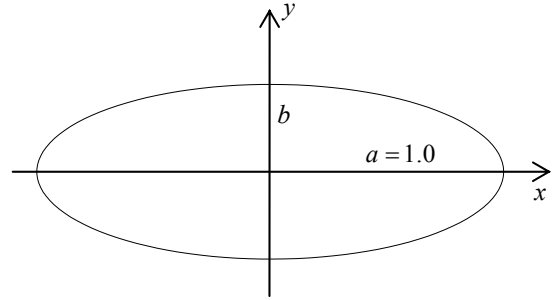


Figure 2: Displacement field problem on an ellipse.

A planar displacement profile is described on the boundary as follows:

$$u_1 = y^3 - 3yx^2 \quad u_2 = -x^3 + 3xy^2.$$

Plane strain cases with Young's modulus  $E=2.5$  (in consistent units) and Poisson's ratio  $\nu=0.3$  has been considered for various ratios  $b/a$ . The relative errors of tractions  $t_1$  and  $t_2$  along the whole boundary (with 44 uniformly spaced sample points) are shown in Figure 3. It can be seen that the solution accuracy of the present RHBNM keeps very high even for the ratio  $b/a$  in the micro-scale.

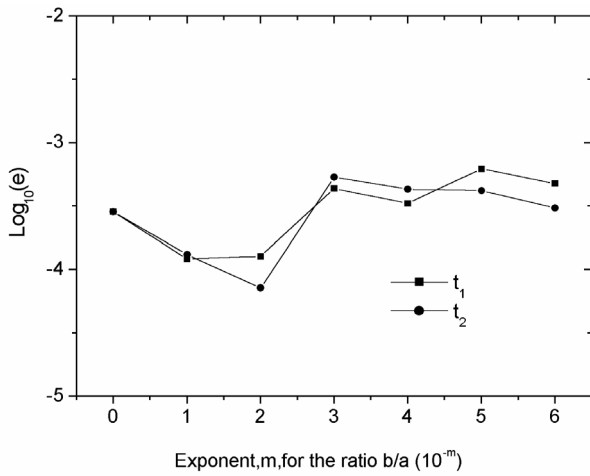


Figure 3: Relative errors of tractions  $t_1$  and  $t_2$  along the boundary for the problem on an ellipse

#### 4.2 Test problem 2: thin coating on a shaft

The second example is taken from Reference [1], of which the geometry is shown in Figure 4. The shaft and coating have outer radii  $r_s$  and  $r_c$  respectively, and two cases are considered here: (a) the thickness  $h = r_c - r_s$  is uniform and approaching to zero while  $r_s$  remains constant, as shown in Figure 4a, and (b) both  $r_s$  and  $r_c$  remain constant, but their centers are misaligned, the normalized eccentricity  $\delta = x_c / (r_c - r_s)$  is shown in Figure 4b. In both cases, uniform pressure  $P$  acts on the outer circumference of the coating, and essential boundary conditions,  $u_1 = u_2 = 0$ , are prescribed around the inner circumference. Plane strain conditions with Young's modulus  $E = 1.92 \times 10^9 Pa$  and Poisson's ratio  $\nu = 0.2$  are assumed and 40 uniformly spaced nodes are used, 20 on the outer circle and 20 the inner circle.

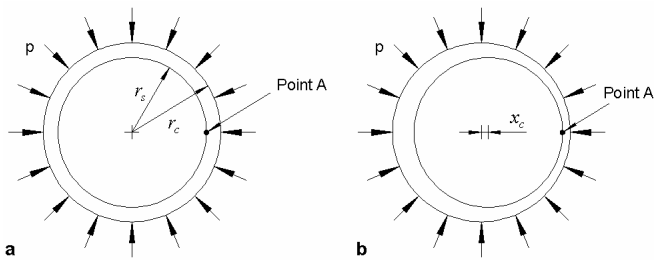


Figure 4: Cross section of a shaft with coatings of **a** uniform and **b** non-uniform thickness.

For the case (a), the relative error of the radial stress  $\sigma_{rr}$  at point  $A$  is shown in Figure 5 while the coating thickness varies in the range of  $10^{-1} r_s \sim 10^{-10} r_s$ . Note that as the coating thickness decreases, the solution accuracy keeps stable and high. Figure 6 shows the normalized radial stress  $\sigma_{rr}$  at point  $A$ , Note that the asymptotic behavior of the RHBNM solution, which approaches the analytical value of the sample problem as  $\delta \rightarrow 0$  (case (a)), and approaches the applied pressure  $p$  as  $\delta \rightarrow 1$ , which is consistent with the physical interpretation, and which is almost the same as that

shown in Reference [1]. Very interesting comparison about the results and the number of nodes used between BEM and FEM can be seen in reference [1] as well.

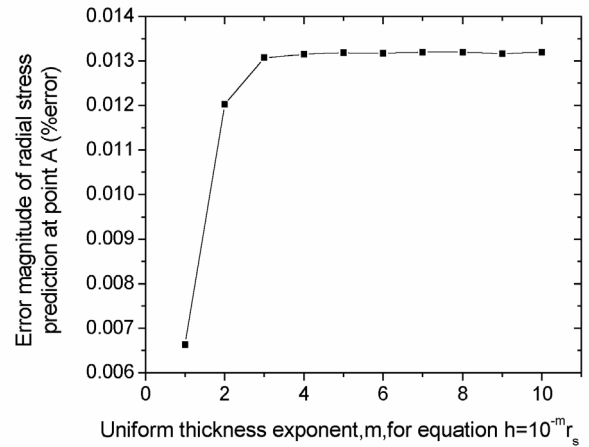


Figure 5: Error magnitude of radial stress at point A for uniform coating thickness.

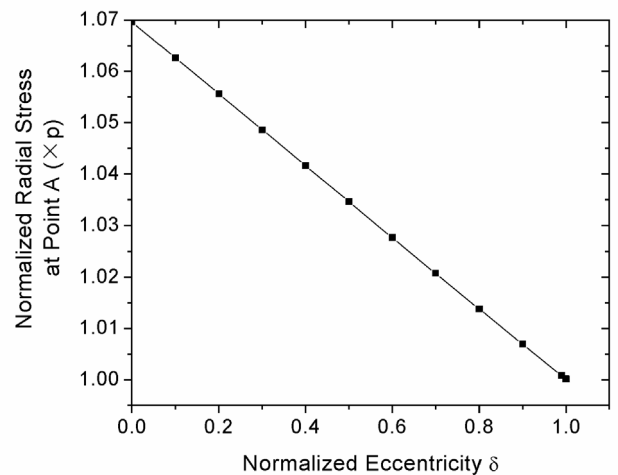


Figure 6: Normalized radial stress at point A for non-uniform coating thickness.

#### 4.3 Test problem 3: linear displacement field problem on an elbow pipe

In order to show the advantages of the truly meshless nature of the RHBNM, another problem of more complicated geometry is added here, which is shown in Figure 7. Since no analytical solution can be found for a practical load case on this structure, to get the accuracy of the RHBNM of this problem, a linear displacement field is considered here. Displacements are prescribed on all faces of the elbow pipe according to the exact solutions. Numerical results of the normal and tangential tractions along the middle ring, together with the exact solutions, are shown in Figure 8. It should be pointed out here that the input file of this problem contains only 339 data!

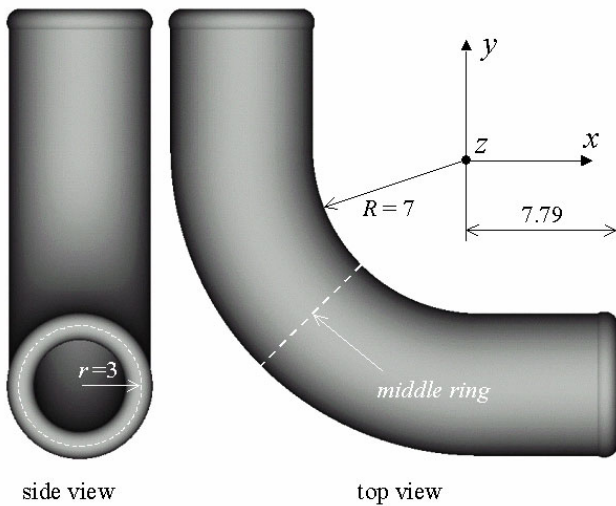


Figure 7: The elbow pipe and its main sizes.

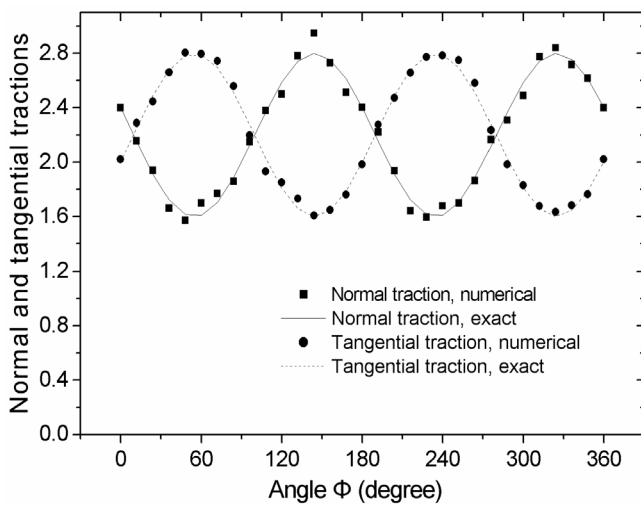


Figure 8: Normal and tangential tractions along the middle ring.

#### 4. Conclusions and Discussion

The applicability of the RHBNM for the analysis of thin shell-like structures has been verified in this paper. The developed RHBNM may provide a very attractive numerical tool for the analysis of thin shell-like structures.

The RHBNM may be more appealing than the BEM due to its meshless nature. It only requires randomly scattered nodal points to be constructed on the bounding surface of a body. Without meshing, it can directly use a solid model for 3-D object. Therefore, the RHBNM may be an important step toward complete analysis automation.

By coupling with the Fast Multipole Method, the RHBNM may be able to solve large complicated structures, such as nano-composite. This is planned in the near future.

#### References

- [1] Luo JF, Liu YJ, Berger EJ. Analysis of two-dimensional thin structures (from micro- to nano-scales) using the boundary element method. *Computational Mechanics*. 1998; 22:404-412.
- [2] Liu YJ. Analysis of shell-like structures by the boundary element method based on 3-D elasticity: formulation and verification. *International Journal for Numerical Methods in Engineering* 1998; 41:541-558.
- [3] Belytchko T, Lu YY, Gu L. Element free Galerkin methods. *International Journal for Numerical Methods in Engineering*. 1994; 37:229-256.
- [4] Zhu T, Zhang J, Atluri SN. A local boundary integral equation (LBIE) method in computation mechanics, and a meshless discretization approach. *Computational Mechanics* 1998; 21:223-235.
- [5] Atluri SN, Zhu T. A new meshless local Petrov-Galerkin approach in computational mechanics. *Computational Mechanics* 1998; 22:117-127
- [6] Mukherjee YX, Mukherjee S. The boundary node method for potential problems. *International Journal for Numerical Methods in Engineering*. 1997; 40:797-815.
- [7] Zhang JM, Yao ZH, Li H. A hybrid boundary node method. *International Journal for Numerical Methods in Engineering*. 2002, 53: 751-763.
- [8] Zhang JM, Yao ZH. A new meshless regular hybrid boundary node method. *Computer Modeling in Engineering & Sciences* 2001; 2:307-318.
- [9] DeFigueredo TGB, Brebbia CA. A new hybrid displacement variational formulation of BEM for elastostatics. Brebbia CA and Conner JJ (eds.), *Advances in Boundary Elements, CMP* 1989; 1:47-57.